Brazilian Journal of Geophysics, **42** (2024), 1, 1–9
Brazilian Geophysical Society
ISSN 2764-8044
DOI 10.22564/brjg.v41i2.2308

ASSESSING TIME-LAPSE FULL-WAVEFORM INVERSION STRATEGIES IN A BRAZILIAN PRE-SALT SETTING

Brenno Hochwart [1*], Sérgio Luiz Eduardo F. da Silva [2],
Marco Cetale [1], and Roger M. Moreira [1]

[1]Universidade Federal Fluminense - UFF, Seismic Inversion and Imaging Group - GISIS, Niterói, RJ, Brazil
[2]Politecnico di Torino, Istituto dei Sistemi Complessi del Consiglio Nazionale delle Ricerche - ISC-CNR, Turin, Italy

*Corresponding author: brennohc@id.uff.br

ABSTRACT. We conducted a comparative study of time-lapse full-waveform inversion (time-lapse FWI) strategies, considering a typical deep-water Brazilian pre-salt setting. This study employed a realistic P-wave model, ocean bottom nodes (OBN) acquisition, noisy data, and a Gaussian anomaly to represent time-lapse model changes. We evaluated the four most commonly used time-lapse FWI schemes. In the first, known as parallel time-lapse FWI, two independent FWI processes are performed from the same initial model, utilizing baseline and monitor datasets. In the second strategy, namely sequential time-lapse FWI, the retrieved baseline model serves as the starting model for inverting monitor data. In both cases, the time-lapse model is derived by subtracting the retrieved baseline model from the retrieved monitor model. The remaining two methods were double-difference and central-difference time-lapse FWI. Our findings demonstrate that all these schemes can detect model variations of 3%. Remarkably, the central-difference time-lapse FWI method demonstrated superior accuracy in producing time-lapse models and, as such, presents itself as a promising strategy for implementation in time-lapse studies within Brazilian pre-salt regions.

Keywords: Time-lapse FWI; Brazilian pre-salt; ocean bottom nodes (OBN); Central-difference FWI; Seismic reservoirs

INTRODUCTION

Characterizing and monitoring reservoirs are vital in strategically planning oil and gas production operations. Time-lapse studies serve as a critical tool for discerning nuanced variations within seismic reservoir properties (Sambo et al., 2020). These variations can be attributed to many factors, including the dynamic processes associated with fluid injection and extraction. Time-lapse investigations delve into the meticulous analysis of geophysical data acquired through two or more distinct seismic surveys conducted at varying temporal intervals within the same geographical area (Lumley, 2001). Through these comparative examinations, geoscientists can understand how subsurface physical properties evolve over time, enabling them to optimize production strategies, enhance hydrocarbon recovery and make informed decisions regarding reservoir management and environmental impact assessments (Nguyen et al., 2015; Cardoso et al., 2022).

Time-lapse approaches operate under the premise that features within the target area exhibit more significant variations from one seismic acquisition to another when contrasted with the surrounding region. Within this context, alterations in the overburden are obtained by analyzing the disparities among each survey conducted in the time-lapse domain. This approach is grounded in the reliable assumption that geological attributes, which remain constant over time and contribute to the seismic image, including factors like lithology, porosity,and shale content, tend to cancel out. Consequently, the remaining changes observed (time-lapse model) are primarily associated to the time-varying dynamic properties associated with, for instance, fluid flows. These dynamic properties encompass alterations in fluid saturation and pore pressure, which are crucial factors to monitor and understand when evaluating the subsurface environment.

However, the issue of non-repeatability (NR) can introduce a significant challenge in obtaining suitable time-lapse models (Borges et al., 2021). NR issues can cause false time-lapse anomalies, which may be mistakenly interpreted as alterations in the physical characteristics of the subsurface (Zhou and Lumley, 2021b). To address this challenge, the deployment of ocean bottom node (OBN) surveys has gained prominence, representing a practical solution to mitigate NR errors (Yang et al., 2016). This shift towards OBN surveys has been driven by the inherent difficulties associated with streamer surveys in managing NR, azimuth illumination, fold and longer offset concerns Cypriano et al. (2019). A case in point is the Tupi Nodes pilot project, a study conducted by Cruz et al. (2021), which underscores the advantages of OBN technology in the context of deep-water Brazilian pre-salt reservoirs. The Tupi Nodes pilot project demonstrated a highly favorable time-lapse response by leveraging full-waveform inversion (FWI) (Virieux and Operto, 2009) as an integral component of the time-lapse seismic processing toolkit. FWI enables precise estimation of rock property changes (Warner et al., 2013; Górszczyk et al., 2021; da Silva et al., 2024), such as P-wave velocity alterations, further enhancing subsurface analysis accuracy in dynamic geological environments. Consequently, operating the FWI technique to analyze OBN data can yield significantly more precise subsurface models.

This work essays a comprehensive comparative analysis of time-lapse FWI methodologies within the context of a typical deep-water Brazilian pre-salt geological setting. Specifically, we consider an OBN acquisition geometry to determine the most effective time-lapse FWI seismic monitoring technique for identifying changes in the properties of ultra-deep reservoirs while contending with noisy data. It is important to emphasize that, owing to the inherent nonlinear characteristics of FWI, our investigation also delves into the nonlinear artifacts introduced by the data inversion process. These artifacts can introduce subsurface model changes unrelated to reservoir variations, as highlighted in prior researches (Yang et al., 2015; Zhou and Lumley, 2021b; da Silva et al., 2023). The choice to employ FWI is rooted in its standing as a robust seismic inversion method that leverages the comprehensive physical principles embedded within a wave equation (Virieux and Operto, 2009). From a practical standpoint, FWI is usually formulated as a local optimization problem, where the primary objective is to minimize the sum of squared differences between the modeled data (derived from the wave equation solution) and the observed seismic data (Fichtner, 2010). Utilizing the entire waveforms, rather than solely travel times or amplitudes, enables a comprehensive evaluation of the propagation of waves that illuminate the subsurface.

Time-lapse seismic methodologies entail the implementation of two distinct seismic surveys within the same geographical area. In the initial survey, known as the baseline data acquisition, baseline data is recorded, while the follow-up surveys record monitor data. In this work we explore the applicability of the four most widely employed time-lapse FWI strategies, considering one monitor data acquisition. The first strategy, *parallel time-lapse FWI* (Lumley, 2001), consists of conducting two independent FWI processes starting from the same initial model. The baseline and monitor models are constructed using the respective baseline and monitor data sets. The time-lapse model is subsequently ascertained by subtracting the retrieved baseline model from the retrieved monitor model. In the second strategy, *sequential time-lapse FWI* (Routh et al., 2012), the retrieved baseline model serves as the starting point for inverting the monitor data. The time-lapse changes are calculated by subtracting the retrieved baseline model from the new retrieved monitor model obtained through the inversion of the monitor data. In the third time-lapse FWI approach, double-difference time-lapse FWI (DDWI) (Yang et al., 2015), the retrieved baseline model serves as the initial model for inverting the difference between the baseline and monitor data sets. The time-lapse changes are derived by subtracting the retrieved baseline model from the new model acquired through this inversion process. Finally, in the fourth time-lapse FWI approach considered in this work, *central-difference time-lapse FWI* (CFWI) (Zhou and Lumley, 2021a), the retrieved baseline and monitor models are employed as initial models for a new FWI application. In particular, the retrieved baseline model is used as the starting model for inverting the monitor model, producing a second monitor model. Simultaneously, the retrieved monitor model is employed as the initial model for inverting the baseline data, creating a second baseline model. The resulting time-lapse model is then computed by subtracting the arithmetic mean of the baseline models from the arithmetic mean of the monitor models.

The structure of this work is as follows: in the subsequent section we briefly present the main ingredients of FWI and the time-lapse schemes employed in this work. Then, in the numerical experiments section, we present our implementation of a 2D acoustic FWI in the time-domain employing a finite difference computational algorithm. Notably, our focus is examining the sensitivity of the aforementioned time-lapse methodologies employing FWI and OBN. Finally, in the last section, we discuss and present our concluding remarks, outlining the best time-lapse strategies and prospects for future research endeavors.

METHODS

Full-waveform inversion (FWI)

Full-waveform inversion (FWI) is a powerful technique that aims to retrieve a high-resolution subsurface model iteratively (Virieux and Operto, 2009). In this approach, an initial model is considered and seismic waveforms are modeled based on this model by numerically solving a wave equation. In this work we assume the premise that the following acoustic wave equation describes the wavefields:

$$\nabla^2 p_s(\vec{x},t) - \frac{1}{m^2(\vec{x})}\frac{\partial^2 p_s(\vec{x},t)}{\partial t^2} = f_s(\vec{x}_s,t), \quad (1)$$

where p_s denotes the modeled wavefield; m represents the P-wave velocities (model parameters) to be estimated; and $f_s(\vec{x}_s,t)$ is a seismic source s fired at the position $\vec{x}=\vec{x}_s$, with $\vec{x}$ and $0 \le t \le T$ representing, respectively, the spatial coordinate and the time; T is the maximum recording time.

Then, these synthetic waveforms (modeled data) are compared with the observed data through an objective function ϕ (Fichtner, 2010). In this work we consider a classical time-domain FWI, in which the objective function is defined as:

$$\phi(m) := \frac{1}{2}\sum_{s,r}\int_0^T \Big(\Gamma_{s,r}p_s(m,t) - d_{s,r}(t)\Big)^2 dt, \quad (2)$$

where $\Gamma_{s,r}p_s$ and $d_{s,r}$ represent modeled and observed data, respectively, in which $\Gamma_{s,r}$ is an extracting operator onto the receiver r of the source s (da Silva et al., 2020).

Due to the FWI non-linearity, model recovery is performed iteratively (Virieux and Operto, 2009). In this work we consider a Fletcher-Reeves nonlinear conjugate gradient method (see, for example, Nocedal and Wright (2006)) to solve the FWI problem. We chose to use this nonlinear conjugate gradient algorithm because it has been shown to work well when analyzing real data from the pre-salt region of Brazil, as recently presented by da Silva et al. (2024). This optimization method involves updating the subsurface model by minimizing an objective function ϕ in the following way:

$$m_{i+1} = m_i - \alpha_i\, h(m_i), \quad \text{for} \quad i = 0,1,2,\cdots,N_{iter}, \quad (3)$$

where N_{iter} represents the maximum number of FWI iterations; $\alpha_i > 0$ denotes the step size Nocedal and Wright (2006); and

$$h(m_i) = \begin{cases} \nabla_m\phi(m_0) & , \; if \;\; i=0 \\ \nabla_m\phi(m_i) + \zeta(m_i)h(m_{i-1}), & \\ \text{for } i = 1,2,\cdots,N_{iter} & \end{cases} \quad (4)$$

is the descent direction; $\nabla_m\phi(m)$ denotes the gradient of the objective function; and

$$\zeta(m_i) = \frac{\nabla_m\phi(m_i)\Big(\nabla_m\phi(m_i) - \nabla_m\phi(m_{i-1})\Big)}{\nabla_m\phi(m_{i-1})\nabla_m\phi(m_{i-1})}. \quad (5)$$

We compute the gradient of the objective function efficiently by applying the adjoint-state method (see, for instance, Plessix (2006)). In this regard, the gradient is obtained by cross-correlating the wavefield p_s with the adjoint-wavefield λ_s, given by (Lailly, 1983):

$$\nabla_m\phi(m) = -\sum_s\int_0^T \lambda_s(T-t)\,\frac{\partial^2 p_s(m,t)}{\partial t^2}\,dt, \quad (6)$$

in which the adjoint-wavefield is obtained by solving

$$\nabla^2\lambda_s(\vec{x},t) - \frac{1}{m^2(\vec{x})}\frac{\partial^2\lambda_s(\vec{x},t)}{\partial t^2} = \sum_r \Gamma^{\dagger}_{s,r} \Big(\Gamma_{s,r}p_s(m,t) - d_{s,r}(t)\Big), \quad (7)$$

which is the adjoint-state wave equation, where $\dagger$ denotes the transpose.

Time-lapse FWI strategies

In this section we present the time-lapse FWI frameworks considered in this work. Time-lapse analyses involve the conduction of two distinct seismic surveys operated within the same geographic region but at varying time intervals. The initial survey yields what we term as the baseline data, denoted as d_b, while the subsequent survey captures the monitor data, labeled as d_m. For a concise notation, we adopt the expression δm to represent the retrieved time-lapse model.

In this work we explore four distinct time-lapse FWI schemes:

(i) **Scheme I:** In the first scheme, also known as the *parallel time-lapse FWI* (Lumley, 2001), we perform two independent FWI procedures from the same initial model, denoted as m_0, where the baseline and monitor seismic data are utilized in these detached inversions. The resulting time-lapse model is derived by subtracting the retrieved baseline model, m_b, from the retrieved monitor model, m_m, denoted as:

$$\delta m_{par} = m_m - m_b. \quad (8)$$

(ii) **Scheme II:** In the second scheme, also known as the *sequential time-lapse FWI* (Routh et al., 2012), we start by obtaining the baseline model, m_b, inverting the baseline data, d_b, by starting from the initial model m_0. Subsequently, a new FWI is conducted, inverting the monitor data d_m by using the retrieved baseline model m_b as the initial model. The resulting time-lapse model is obtained from

$$\delta m_{seq} = m'_m - m_b, \tag{9}$$

where m'_m represents the retrieved monitor model when initiated from m_b.

(iii) **Scheme III:** In the third scheme, also known as the double-difference time-lapse FWI (DDWI) (Yang et al., 2015), we first obtain the baseline model, m_b, inverting the baseline data, d_b, from the initial model m_0. Subsequently, a new FWI is conducted, starting from the retrieved baseline model m_b and inverting the difference between the double-difference: $\delta d(m_{dd}, t) = \left[\Gamma_{s,r} p_{s_b}(m_b, t) - \Gamma_{s,r} p_{s_{dd}}\right] - \left[d_b(t) - d_m(t)\right]$, where $\Gamma_{s,r} p_{s_b}(m_b, t)$ and $\Gamma_{s,r} p_{s_{dd}}(m_{dd}, t)$ are the modeled data from the retrieved baseline model, m_b, and the model m_{dd} to be reconstructed, respectively. The resulting time-lapse model is then obtained through

$$\delta m_{dd} = m_{dd} - m_b, \tag{10}$$

with m_{dd} representing the resulting model from the inversion of the observed data difference, $d_b(t) - d_m(t)$, to the modeled data difference, $\Gamma_{s,r} p_{s_b}(m_b, t) - \Gamma_{s,r} p_{s_{dd}}$, starting from the model m_b.

(iv) **Scheme IV:** In the last scheme, also known as the *central-difference time-lapse FWI* (Zhou and Lumley, 2021a), we conduce two independent FWI processes starting from the model m_0, using the baseline and monitor seismic data to retrieve the baseline m_b and monitor m_m models, in a manner akin to the *parallel time-lapse FWI* strategy. This is the first step. The second step also involves two FWI procedures, closely resembling the *sequential time-lapse FWI* strategy, with one using the monitor data d_m and initiating from m_b to establish a new monitor model m'_m. The other utilizes the baseline data d_b and starting from m_m to generate a new base model m'_b. Then, the resulting time-lapse model is obtained from the average of the differences between the monitor and baseline models from both steps, specifically

$$\delta m_{cd} = \frac{m_m + m'_m}{2} - \frac{m_b + m'_b}{2}. \tag{11}$$

Figure 1 provides a graphical representation summarizing these time-lapse strategies, shedding a comprehensive understanding of the workflows of these time-lapse FWI schemes.

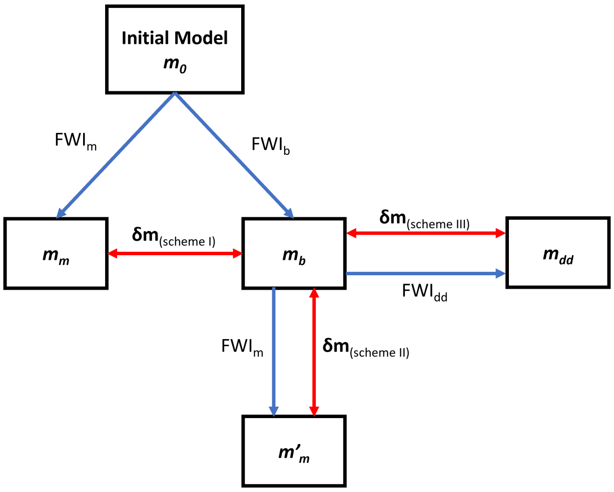

Figure 1: Inversion workflow. Starting from the initial model m_0, we obtain m_b and m_m. From m_b, we then recover m_{dd} and m'_m. Here, FWI stands for a time-invariant FWI while the FWI subscripts refer to the observed data used, with m representing the monitor; b, the baseline; and dd, the observed data difference $d_m - d_b$ used in the Double-Difference Waveform Inversion.

NUMERICAL EXPERIMENTS

In order to conduct a comparative assessment of the time-lapse FWI schemes, we consider a realistic Brazilian pre-salt P-wave velocity model, as initially modified from Karsou (2020), which is depicted in Figure 2a. This model encompasses a geological structure featuring a deep-water layer, with an average depth of 2km, underlying post-salt marine shales and rock layers, a substantial salt body, a pre-salt oil reservoir and bedrock below. We discretize this P-wave model into a regular grid comprising 840 × 280 points, with each cell measuring 25 × 25m. We adopt an OBN geometry for data acquisition in all numerical experiments. This geometry comprises 23 nodes situated on the ocean floor, spaced at intervals of $400m$ (indicated by white triangles in Figure 2a), along with 257 seismic sources positioned at a depth of $10m$ (marked by the green line in Figure 2a) and separated by 50m apart. The seismic source employed was a Ricker wavelet with a peak frequency of 5Hz. We set to 7s the acquisition time.

Using the P-wave model presented in Figure 2a, we generate the baseline data set d_b by employing the 2D time-domain acoustic wave equation (1). Subsequently, we introduce Gaussian noise with a signal-to-noise ratio (SNR) of 10dB to mimic real-world conditions. Moreover, we perturb the baseline model by introducing a bivariate Gaussian anomaly to construct the monitor model, as depicted in Figure 2c. In this context, we simulate a time-lapse model featuring a maximum P-wave velocity reduction of 3% at the reservoir level. While the differences between the monitor and baseline true models might not be readily discernible to the naked eye, denoting it as the true time-lapse model. With the monitor model in place, we then generate the monitor data d_m using the 2D time-domain acoustic wave equation (1) and subsequently apply Gaussian noise with an SNR of 10dB. In Figure 3, Panels (a) and (b) depict receiver-gathers corresponding to the first node from the baseline and monitor models, respectively, while Panel (c) highlights the difference between these seismograms.

To solve the FWI problem, we consider a scaling factor of 0.05, following the recommendation by Köhn (2011). We set the stopping criterion for our numerical simulations at 50 iterations. To avoid drastic effects caused by cycle-skipping issues (Hu et al., 2018), we consider that the initial model m_0 was well determined from a kinetic point of view. In particular, we generate the initial model m_0 by smoothing the true model (Figure 2a) with a Gaussian operator with a standard deviation of $250m$. The model m_0 is depicted in Figure 2b. Figure 4 shows the retrieved FWI models. The FWI results exhibit remarkable similarity; thus, the minimal dissimilarities are only discernible in the time-lapse domain. Figure 5 shows the resulting time-lapse models associated with the four time-lapse FWI schemes. Within this visual representation, a notable observation emerges regarding *Scheme II*, where the resulting time-lapse model is predominantly marked by artifacts throughout the model, as showcased in Figure 5b. Unfortunately, this outcome falls short of expectations, as it deviates significantly from the true time-lapse model (Figure 2c). *Scheme III* also exhibits several artifacts, albeit on a smaller scale, particularly near the upper regions of the salt layer. In contrast, *Scheme I* and *Scheme IV* demonstrate a more effective mitigation of the time-lapse noises from the ocean floor and the uppermost salt layer. Furthermore, it is crucial to recognize that, within *Scheme I* and *Scheme IV*, certain artifacts do exist; however, their presence is unrelated to geological structures, as seen in *Scheme II* and *Scheme III.* Instead, these artifacts are primarily associated with noise in the central portion of the model, spanning distances between 5 and 15 km, and mark the wavepaths at the extremeties of the model where seismic illumination is practically absent.

Figure 6 shows P-wave vertical-velocity profiles depicting model changes arising from the time-lapse FWI schemes against the true time-lapse model represented by the black curve. These profiles are observed at distinct distances: 10.25km, 10.50km (the central region of the Gaussian anomaly) and 10.75km. All the schemes can detect time-lapse changes within the pre-salt reservoir. Nevertheless, *Scheme II* exhibits heightened discrepancies when evaluating regions beyond the primary target area. This is evident from larger amplitude variations around $\delta m = 0$, which suggests pronounced errors relative to *Schemes I*, *III* and *IV.* Furthermore, *Scheme II* appears to overreach in estimating time-lapse changes, as indicated by the purple curve. On a brighter note, the efficacy of *Schemes I*, *III* and *IV* is highlighted by their adeptness at identifying the time-lapse changes, particularly within depths ranging from 5.5 to 6.0 km. Notably, *Scheme IV* outperforms the rest in its remarkable precision within the area of peak seismic illumination (central segment of the P-wave model). This prowess is noted through the almost perfect alignment of the blue curve (representing *Scheme IV*) with the benchmark black curve in the pre-salt domain, as showcased in Figure 6(b).

CONCLUSIONS

In this work we have compared the most used time-lapse FWI methodologies in the literature, drawing inspiration from the challenging ultra-deep reservoirs from the Brazilian pre-salt oil region. Our findings have unveiled the potentialities and difficulties of these time-lapse strategies in detecting subtle changes in P-wave velocity within a typical Brazilian pre-salt oil reservoir, all while utilizing cutting-edge OBN technology. Importantly, it is worth noting that the inversion artifacts exhibited distinctive behaviors across the various time-lapse FWI schemes we investigated.

Within the Brazilian pre-salt case study, *Scheme I* (parallel time-lapse FWI) and *Scheme IV* (central-difference time-lapse FWI) have emerged as promising strategies, providing robust and accurate time-lapse responses, even when analyzing noisy data. These two strategies have effectively represented the expected time-lapse model changes, as depicted in Figure 5. On the other hand, while yielding satisfactory results, *Scheme III* has shown a tendency to introduce significant artifacts at the top of the salt layer. These artifacts, while intriguing, could potentially lead to misleading geophysical interpretations. *Scheme II*, however, has presented some limitations, as it introduces time-lapse changes across the entire P-wave model, not solely related to reservoir production.

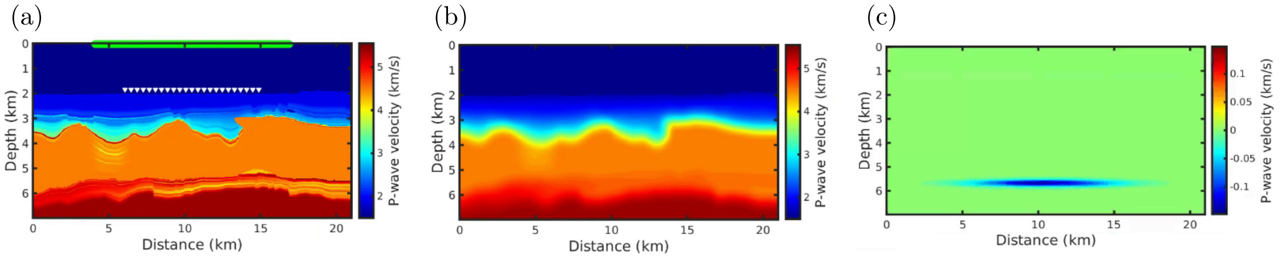

Figure 2: (a) Typical Brazilian pre-salt P-wave velocity model and OBN acquisition, where the white triangles represent the nodes and the green line are the shot points. (b) Initial model m_0. (c) True time-lapse model changes.

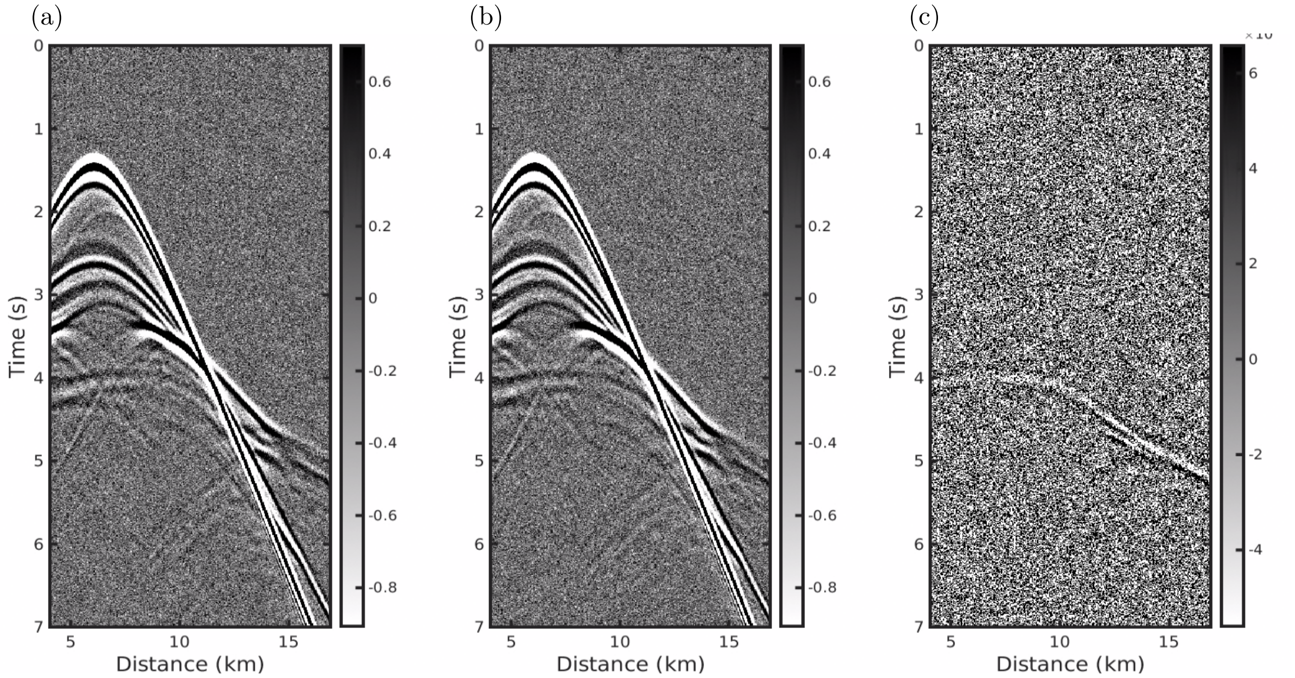

Figure 3: Observed seismograms. (a) Baseline data, d_b. (b) Monitor data, d_m. (c) Difference between monitor and baseline data, $d_m - d_b$.

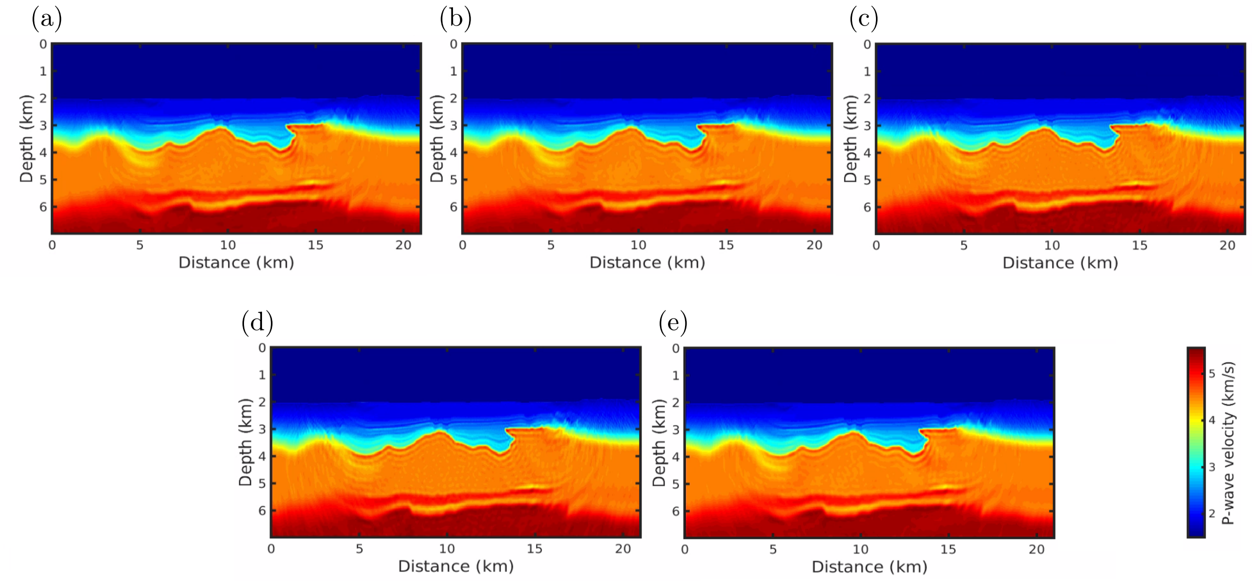

Figure 4: FWI resulting models: (a) Retrieved baseline model, m_b, and (b) retrieved monitor model, m_m. Retrieved (c) monitor model m'_m from baseline model m_b, and (d) retrieved baseline model m'_b from monitor model m_m. (e) Retrieved DDWI model m_{dd} from baseline model m_b using double-difference data.

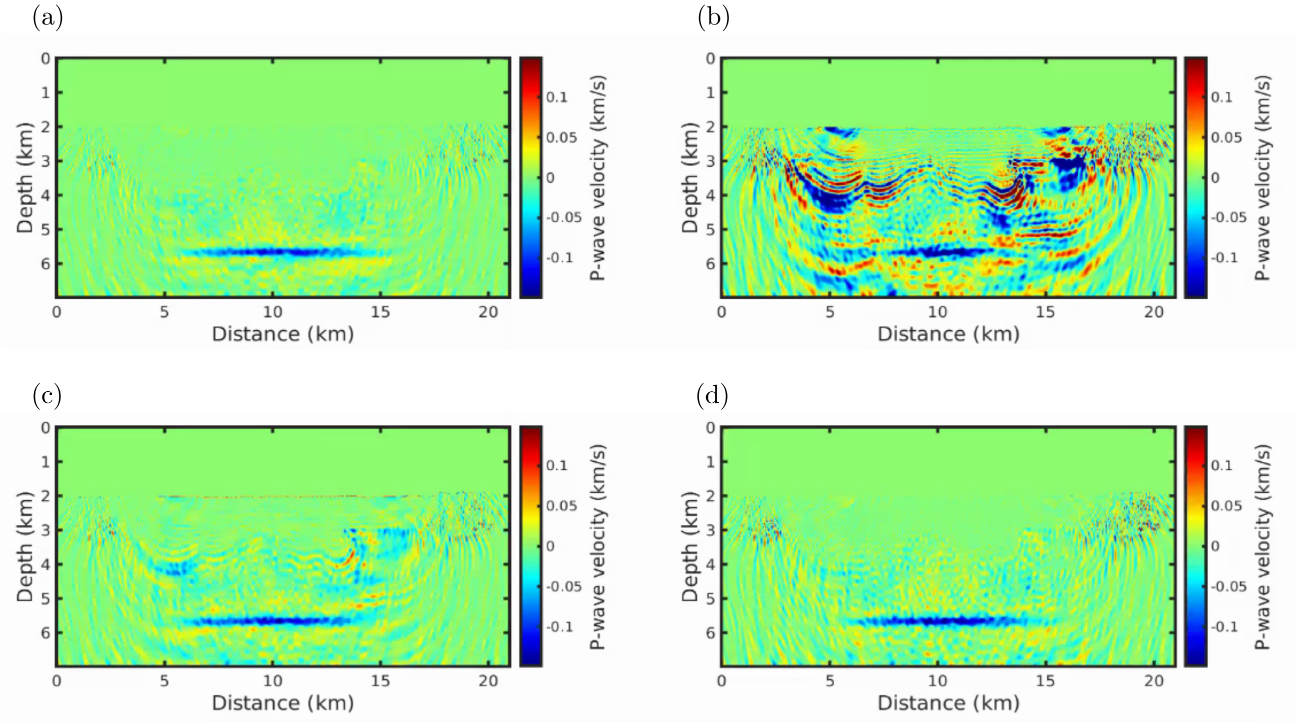

Figure 5: Recovered time-lapse model changes from: (a) *Scheme I*, (b) *Scheme II*, (c) *Scheme III* (DDWI) and (d) *Scheme IV* (CFWI).

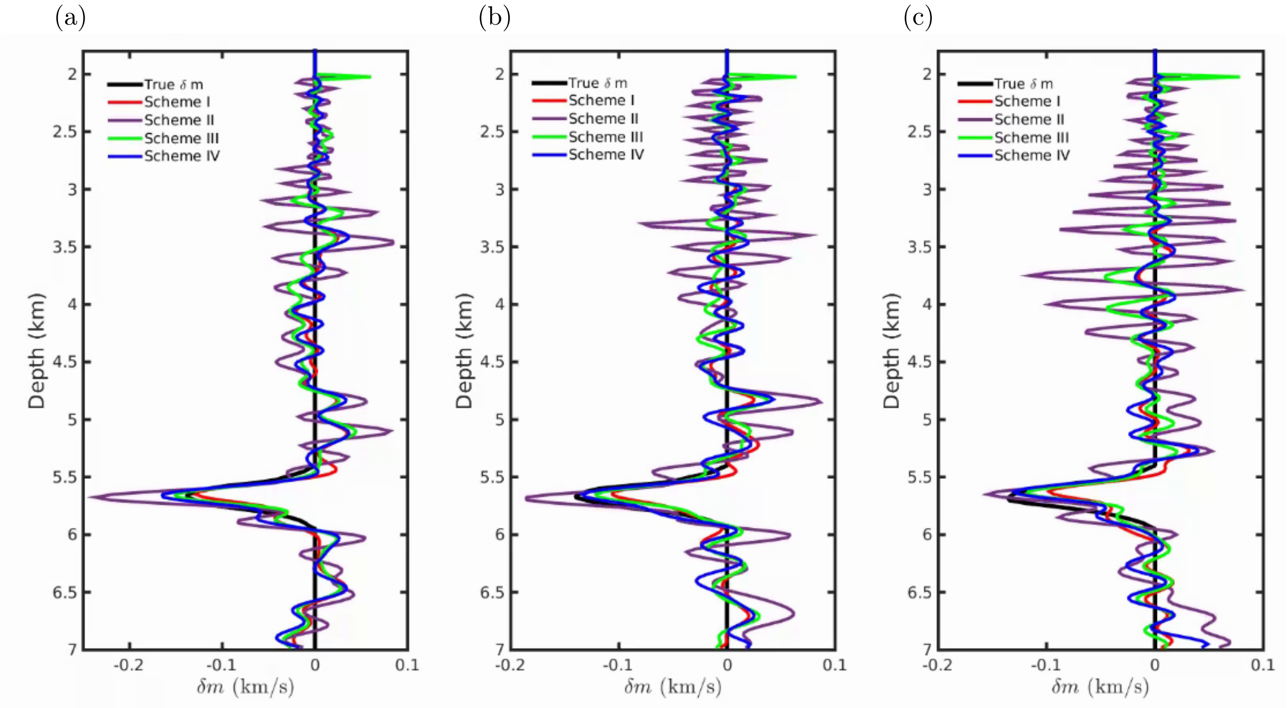

Figure 6: P-wave vertical-velocity profiles for the time-lapse schemes at a lateral distance of: (a) 10.25km, (b) 10.50km and (c) 10.75km.

This scheme led to a higher incidence of changes in the overburden and possibly spurious correlations linked to noise. From a computational perspective, the complexity of these schemes is intricately related to the number of inversions conducted within each proposed workflow. *Scheme I*, *Scheme II* and *Scheme III* exhibit comparable computational efforts, with the additional misfit data in *Scheme III* constituting a computationally trivial aspect. Conversely, *Scheme IV* entails two extra inversions compared to the previous schemes, necessitating more substantial computational resources.

Our future endeavors are poised to explore the resilience of these four strategies concerning non-repeatability (NR) effects, encompassing factors such as water velocity variations and errors in shot-receiver positioning. Furthermore, we aim to model the complexities of wave physics, incorporating effects related to density and shear velocity. These endeavors will undoubtedly contribute to a more comprehensive understanding of time-lapse FWI methodologies and their adaptability in challenging geological settings.

REFERENCES

Borges, F., M. Muzzette, L. E. Queiroz, B. Pereira-Dias, R. Dias, and A. Bulcão, 2021, Impact of the non-repeatability of sources and receivers in ocean bottom acquisitions - a synthetic 2D study in Santos basin pre-salt: Brazilian Journal of Geophysics, **39**, 287–294, doi: 10.22564/rbgf.v39i2.2105.

Cardoso, C. A. R., F. S. de Moraes, and K. T. de Pereira e Lima, 2022, Analysis of 4D seismic timeshifts overburden and its relation with the geomechanical model of reservoirs in a Campos basin field: Brazilian Journal of Geophysics, **40**, 371–394, doi: 10.22564/brjg.v40i3.2174.

Cruz, N. M., J. M. Cruz, L. M. Teixeira, M. M. da Costa, L. B. de Oliveira, E. N. Urasaki, T. P. Bispo, M. de Sá Jardim, M. H. Grochau, and A. Maul, 2021, Tupi Nodes pilot: A successful 4D seismic case for Brazilian presalt reservoirs: The Leading Edge, **40**, 886–896, doi: 10.1190/tle40120886.1.

Cypriano, L., Z. Yu, D. Ferreira, B. Huard, R. Pereira, F. Jouno, A. Khalil, E. Urasaki, N. da Cruz, A. Yin, D. Clarke, and C. Cardeal, 2019, OBN for pre-salt imaging and reservoir monitoring—Potential and road ahead: Presented at the 16th International Congress of the Brazilian Geophysical Society, Rio de Janeiro, Brazil. doi: 10.22564/16cisbgf2019.318.

da Silva, S., R. Moreira, B. Hochwart, and M. Cetale, 2023, Suppressing 4D-noise induced by coordinate inaccuracies using a receiver-extension FWI strategy: In Proceedings of the of 84th EAGE Annual Conference & Exhibition, Vienna, Austria, **2023**, 1–5, doi: 10.3997/2214-4609.2023101497.

da Silva, S. L., F. Costa, A. Karsou, F. Capuzzo, R. Moreira, J. Lopez, and M. Cetale, 2024, Research note: Application of refraction full-waveform inversion of ocean bottom node data using a squared-slowness model parameterization: Geophysical Prospecting, **72**, 1189–1195, doi: 10.1111/1365-2478.13454.

da Silva, S. L. E. F., P. T. C. Carvalho, C. A. N. da Costa, J. M. de Araújo, and G. Corso, 2020, An objective function for full-waveform inversion based on frequency-dependent offset-preconditioning: PLOS ONE, **15**, e0240999, doi: 10.1371/journal.pone.0240999.

Fichtner, A., 2010, Full seismic waveform modelling and inversion: Springer Berlin, Heidelberg, 343 pp., doi: 10.1007/978-3-642-15807-0,.

Górszczyk, A., R. Brossier, and L. Métivier, 2021, Graph-space optimal transport concept for time-domain full-waveform inversion of ocean-bottom seismometer data: Nankai trough velocity structure reconstructed from a 1d model: Journal of Geophysical Research: Solid Earth, **126**, e2020JB021504, doi: 10.1029/2020JB021504.

Hu, W., J. Chen, J. Liu, and A. Abubakar, 2018, Retrieving Low Wavenumber Information in FWI: An Overview of the Cycle-Skipping Phenomenon and Solutions: IEEE Signal Process. Mag., **35**, 132–141, doi: 10.1109/MSP.2017.2779165.

Karsou, A. A., 2020, Aceleração dos algoritmos de modelagem acústica e elástica e da inversão do campo de onda completo (FWI) em GPU utilizando OPENACC: Master Dissertation, Universidade Federal Fluminense, Niterói, Brazil.

Köhn, D., 2011, Time domain 2D elastic full waveform tomography: Ph.D. Thesis, Christian-Albrechts Universität Kiel, Kiel, Germany.

Lailly, P., 1983, The seismic inverse problem as a sequence of before stack migration: in Proc. of Conf. on Inverse Scattering, Theory and Applications, SIAM, Philadelphia, Pennsylvania.

Lumley, D. E., 2001, Time-lapse seismic reservoir monitoring: Geophysics, **66**, 50–53, doi: 10.1190/1.1444921.

Nguyen, P. K. T., M. J. Nam, and C. Park, 2015, A review on time-lapse seismic data processing and interpretation: Geosciences Journal, **19**, 375–392, doi: 10.1007/s12303-014-0054-2.

Nocedal, J., and S. J. Wright, 2006, Numerical optimization: Springer, New York, NY, USA.

Plessix, R.-E., 2006, A review of the adjoint-state method for computing the gradient of a functional with geophysical applications: Geophysical Journal International, **167**, 495–503, doi: 10.1111/j.1365-246X.2006.02978.x.

Routh, P., G. Palacharla, I. Chikichev, and S. Lazaratos, 2012, Full wavefield inversion of time-lapse data for improved imaging and reservoir characterization: In: SEG Technical Program Expanded Abstracts 2012, 1–6, doi: 10.1190/segam2012-1043.1.

Sambo, C., C. C. Iferobia, A. A. Babasafari, S. Rezaei, and O. A. Akanni, 2020, The Role of Time Lapse(4D) Seismic Technology as Reservoir Monitoring and Surveillance Tool: A Comprehensive Review: Journal of Natural Gas Science and Engineering, **80**, 103312, doi: 10.1016/j.jngse.2020.103312,.

Virieux, J., and S. Operto, 2009, An overview of full-waveform inversion in exploration geophysics: Geophysics, **74**, WCC1–WCC26, doi: 10.1190/1.3238367.

Warner, M., A. Ratcliffe, T. Nangoo, J. Morgan, A. Umpleby, N. Shah, V. Vinje, I. Štekl, L. Guasch, C. Win, G. Conroy, and A. Bertrand, 2013, Anisotropic 3D full-waveform inversion: Geophysics, **78**, R59–R80, doi: 10.1190/geo2012-0338.1.

Yang, D., F. Liu, S. Morton, A. Malcolm, and M. Fehler, 2016, Time-lapse full-waveform inversion with ocean-bottom-cable data: Application on Valhall field: Geophysics, **81**, R225–R235, doi: 10.1190/geo2015-0345.1.

Yang, D., M. Meadows, P. Inderwiesen, J. Landa, A. Malcolm, and M. Fehler, 2015, Double-difference waveform inversion: Feasibility and robustness study with pressure data: Geophysics, **80**, M129–M141, doi: 10.1190/geo2014-0489.1.

Zhou, W., and D. Lumley, 2021a, Central-difference time-lapse 4D seismic full-waveform inversion: Geophysics, **86**, R161–R172, doi: 10.1190/geo2019-0834.1.

Zhou, W., and D. Lumley, 2021b, Nonrepeatability effects on time-lapse 4D seismic full-waveform inversion for ocean-bottom node data: Geophysics, **86**, R547–R561, doi: 10.1190/geo2020-0577.1.

Hochwart, B.: Data gathering, analysis and interpreting and manuscript writing; **da Silva, S.L.E.F.:** research planning, data analysis, results validation, manuscript writing and revision; **Cetale, M.:** research planning, results discussion and validation and manuscript revision; **Moreira, R.M.:** Research planning, results discussion and validation and manuscript revision.

Received on November 30, 2023 / Accepted on March 19, 2024